SCIENTIFIC Publishing Limited

Journal of Intelligent Communication
http://ojs.ukscip.com/index.php/jic

Article

Fractal Dimension (D_f) Theory of Ismail's Entropy (IE) with Potential D_f Applications to Structural Engineering

Ismail A Mageed *

School of Computer Science, AI, and Electronics, Faculty of Digital Technologies, University of Bradford, BD7 1DP, Bradford, UK
* Correspondence: drismail664@gmail.com

Received: 16 April 2024; **Revised**: 23 July 2024; **Accepted**: 26 July 2024; **Published**: 31 July 2024

Abstract: As an ultimate generalisation to several kinds of generalised entropy in the literature, a novel entropy measure, namely, Ismail's entropy, or (IE), is presented. This article spotlights the significance of fractal dimension, through highlighting several possible applications of fractal dimension to structural engineering. In addition to several difficult open problems and the next step of inquiry, the paper ends with some concluding observations.

Keywords: information theory; structural engineering

1. Introduction

The Shannonian entropy, $H(X)$ in 1948 [1], is obtained by Equation (1):

$$H(X) = \sum_i p(x_i) I(x_i) = -\sum_i p(x_i)\, ln\,(p(x_i)) \quad (1)$$

where the probability of the i^{th} event is given by $p(x_i)$.

Ismail's entropy, namely, IE [2] reads in Equation (2):

$$H_{(q,UG)} = \sum_{n=0}^{N} \varphi((p(n)^q, a_1, a_2, \ldots, a_k)\,, k \le n \quad (2)$$

where φ serves as any well-defined function, $a_1, a_2, \ldots, a_k, k \le n$ serves as any universal parameter, $0.5 < q < 1$.

Selecting the choice, as in Equation (3):

$$\varphi\big((p(n)^q, a_1, a_2, \ldots, a_k\big) = \frac{1}{1-q}(p(n)^q - \frac{1}{n}) \quad (3)$$

generates the Tsallisian Entropy [3], as given by Equation (4),

$$H_T^q\big(p(n)\big) = \frac{1}{1-q}(\sum_{n=0}^{N} \big(p(n)\big)^q - 1) \quad (4)$$

and $q \to 1$, H_T^q generates $H(X)$.

There are several formal definitions that could be used, according to [4–10]. Among the calculations used in such a definition are those that link the fractal dimension (D_f), the scaling factor (ε), and the number of sticks (N) needed to cover a shoreline. Regarding fractal patterns in spatial dimensions, these formulas aid in quantifying their complexity and scaling characteristics, as in Figure 1. D_f is depicted by Equation (5):

$$N \propto \varepsilon^{-D_f} \tag{5}$$

Simplified by Equation (6), to be:

$$ln\, N = - D_f = \frac{ln\, N}{ln\, \varepsilon} \tag{6}$$

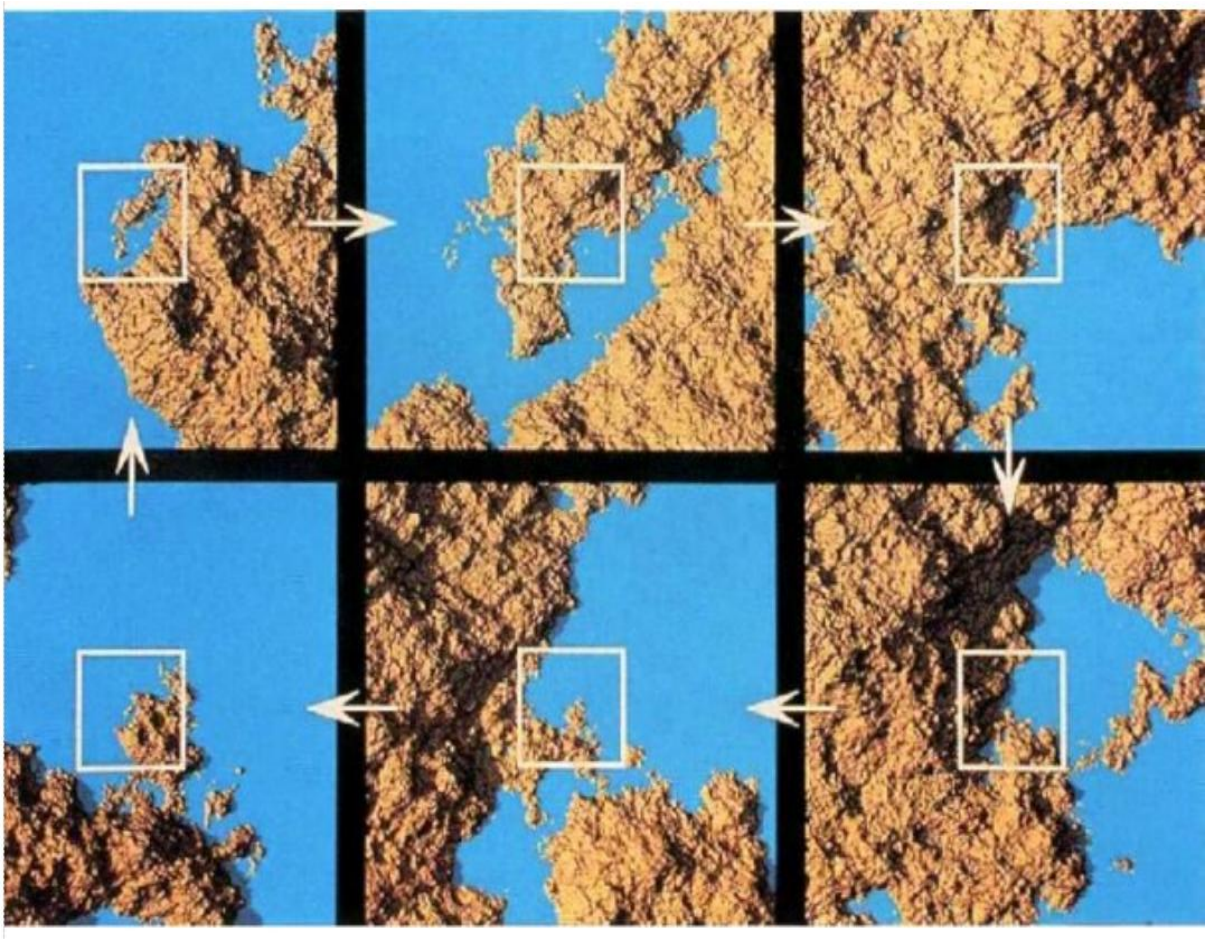

Figure 1. Using Google Earth satellite imagery and the GNU Image Manipulation Programme [10].

A fractal set or fractal [4–10] can be used to illustrate a pattern that occurs naturally, for example, the surface of a broccoli. A fractal is a geometric entity that has a fractional, or non-integer, dimension; the fractal dimension, or D_f, is another name for this fractional dimension. A useful characteristic for categorising fractals is the fractal dimension, which is a generalisation of the conventional idea of a system's dimensionality. A curved line's fractal dimension can be thought of as a measurement of the space filling properties of the line. When oscillations are added to a straight line, their dimension can be thought of as changing from one to two. A flat surface has two dimensions.

We know intuitively that we can attempt to fit a polygon to the contour of an irregular 2D shape to acquire an accurate estimate of its perimeter length P, provided that the polygon's side has a very short and fixed length L. According to theory, the smaller L, the better the approximation of P. If the shape is fractal, on the other hand, we will discover the contradiction that, rather than converging to a fixed value, the perimeter length increases indefinitely when the side lengths get smaller.

In Figure 2, a dramatic heavy-tailed decline of ε is visualized. Yet, another variable, is observed due to the progressive growth of N (a variable). Notably, Figure 3 reveals that ε and another variable decrease simultaneously. More precisely, the progressive increase in the number of used sticks will impact the scaling

factor to decrease dramatically, as in Figure 2, whereas the opposite case appears in connection with fractal dimension, as in Figure 3.

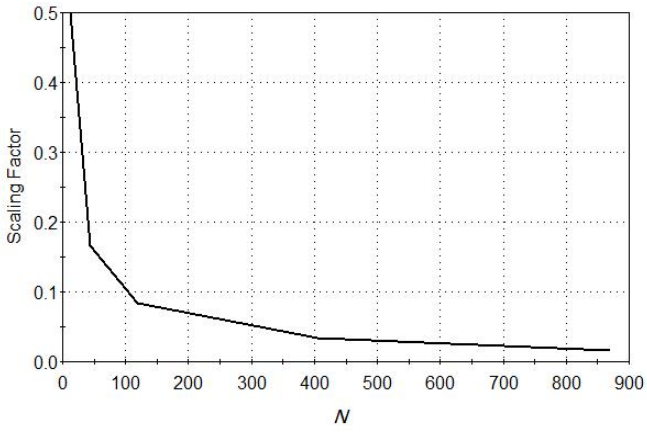

Figure 2. Impact of N on scaling factor.

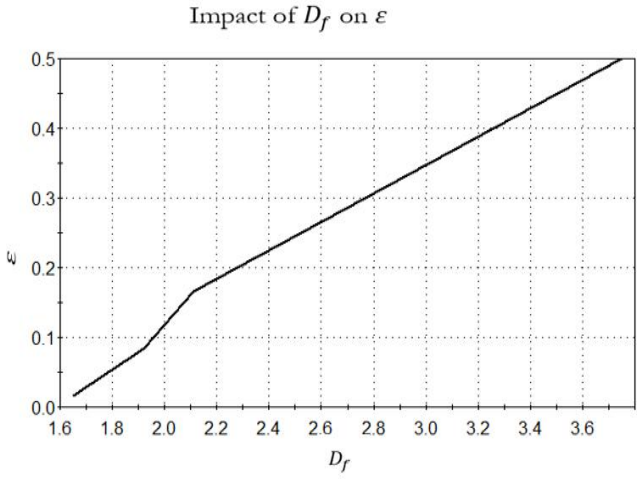

Figure 3. Impact of D_f on ε.

This paper is visualized by Figure 4.

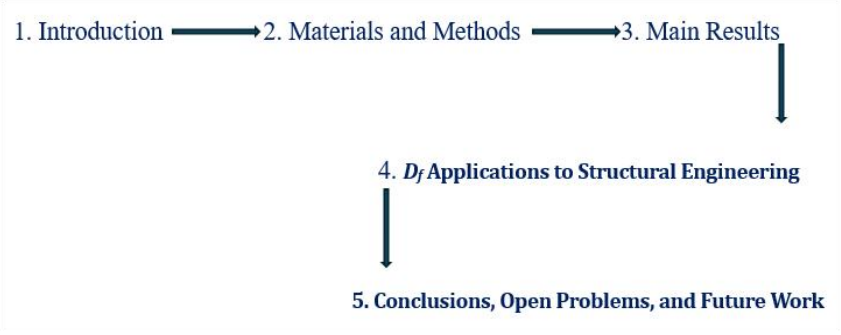

Figure 4. Schematic of the current paper.

2. Materials and Methods

Some entropic dimensions [3,10–15] are calculated, based on $p(i) = \frac{1}{N}$.

The Shannonian dimension [10] rewrites, accordingly to Equation (7) to:

$$D_s = \lim_{\varepsilon \to 0} \frac{ln\, N}{ln \frac{1}{\varepsilon}} \tag{7}$$

The Rényian dimension [12] follows Equation (8):

$$D_R = \lim_{\varepsilon \to 0} \frac{ln\, N}{ln \frac{1}{\varepsilon}} \tag{8}$$

3. Main Results

Theorem 1

For IE (c.f., Equation (2), D_f(IE)) reads by Equation (9):

$$D_f(\text{IE}) = \lim_{\varepsilon \to 0} \frac{N\varphi\left(N^{-q}, a_1, a_{2,}, \ldots, a_k\right)}{ln \frac{1}{\varepsilon}}, k \leq N \tag{9}$$

Proof

It can be seen from Equation (10), that

$$\begin{aligned} D_f(\text{IE}) &= \lim_{\varepsilon \to 0} \frac{\sum_{n=1}^{N} \varphi((\frac{1}{N})^q, a_1, a_{2,}, \ldots, a_k)}{ln \frac{1}{\varepsilon}}, k \leq N \\ &= \lim_{\varepsilon \to 0} \frac{\sum_{n=1}^{N} \varphi(N^{-q}, a_1, a_{2,}, \ldots, a_k)}{ln \frac{1}{\varepsilon}} \end{aligned} \tag{10}$$

following mathematical analysis, $\varphi(N^{-q}, a_1, a_{2,}, \ldots, a_k)$ is not a function of n, which implies by Equation (11):

$$\sum_{n=1}^{N} \varphi(N^{-q}, a_1, a_{2,}, \ldots, a_k) = \varphi\left(N^{-q}, a_1, a_{2,}, \ldots, a_k\right) \sum_{n=1}^{N} 1 = N\varphi(N^{-q}, a_1, a_{2,}, \ldots, a_k) \tag{11}$$

Communicating Equation (12), we have:

$$D_f(\text{IE}) = \lim_{\varepsilon \to 0} \frac{N\varphi(N^{-q}, a_1, a_{2,}, \ldots, a_k)}{ln \frac{1}{\varepsilon}} \tag{12}$$

The obtained results (c.f., reference [2]) are obviously spotlighting the dominance of its own kind of contribution, as follows:

- The special case, $b = G(q, a_1, a_{2,}, \ldots, a_k) = \frac{q}{2-q}, q \in (0, 1), q = \frac{1-k}{1+k}$,corresponds to the NME Kaniadakisian entropic formalism of the stable $M/G/1$ queuing system.
- The special case, $b = G(q, a_1, a_{2,}, \ldots, a_k) = \frac{\tau_s ln(r(0))}{ln \tau_s}$, τ_s =2/(1+ $C_{s,1,S}^2$) corresponding to the KL entropy formalism of the stable $M/G/1$ queue.
- The special case, $b = G\left(q, a_1, a_{2,}, \ldots, a_k\right) = \frac{ln\left(\frac{\tau_S}{\xi(\delta,n)}\right)}{q ln \tau_s}$; δ is the geometric parameter; satisfying that $\delta > 1$, τ_s=2/(1+$C_{s,1,S}^2$), $\xi(\delta, n)$ is the well-known Hurwiz-Rienmannian Zeta function, as in Equation (13).

$$\xi(\delta, n)e = \sum_{n=1}^{\infty} n^{-s} \tag{13}$$

The power of Theorem 1 is manifested within the following corollary.

Corollary 2

D_f (IE) reduces to $D_{Z_{a,b}}$ entropy [4], satisfying Equation (14):

$$D_{Z_{a,b}} = \lim_{\varepsilon \to 0} \frac{\frac{1}{(1-q)(a-b)}\left(N^{(1-q)a} - N^{(1-q)b}\right)}{ln\frac{1}{\varepsilon}} \tag{14}$$

provided that, $0.5 < q < 1, a > 1, b \in \mathbb{R}$ or $b > 0, a \in \mathbb{R}$ with $a \neq b$.

Proof

Choosing the mathematical convention, as in Equation (15):

$$\varphi\left(N^{-q}, a_1, a_{2,}, \ldots, a_k\right) = \frac{1}{(1-q)(a-b)N}\left[(N^{1-q})^a - (N^{1-q})^b\right] \tag{15}$$

Such that Equation (16) holds:

$$a_1 = \frac{1}{N(1-q)(a-b)}, a_2 = a_3 = \ldots = a_N = 0 \tag{16}$$

We are now to prove that $\varphi\left(N^{-q}, a_1, a_{2,}, \ldots, a_k\right)$ (c.f., Equation (15)) is well-defined. To do so, following Equation (15), let $N_1 \neq N_2$, to satisfy Equation (17):

$$\frac{1}{(1-q)(a-b)}\left[\left((N_1)^{a(1-q)-1}\right) - \left((N_1)^{b(1-q)-1}\right)\right] = \frac{1}{(1-q)(a-b)}\left[\left((N_2)^{a(1-q)-1}\right) - \left((N_2)^{b(1-q)-1}\right)\right] \tag{17}$$

Hence, by Equation (18):

$$\left[\left((N_1)^{a(1-q)-1}\right) - \left((N_1)^{b(1-q)-1}\right)\right] = \left[\left((N_2)^{a(1-q)-1}\right) - \left((N_2)^{b(1-q)-1}\right)\right] \tag{18}$$

Accordingly, by Equation (19):

$$\left[\left((N_1)^{\alpha}\right) - \left((N_2)^{\alpha}\right)\right] = \left[\left((N_1)^{\beta}\right) - \left((N_2)^{\beta}\right)\right] \tag{19}$$

Such that Equation (20) holds:

$$\alpha = a(1-q) - 1, \beta = b(1-q) - 1 \tag{20}$$

Engaging mathematical analysis and Equation (16), we get to Equation (21):

$$(N_1 - N_2)\begin{bmatrix} (N_1)^{\alpha-1} + (N_1)^{\alpha-1}N_2 + \ldots + (N_2)^{\alpha-1} \\ + (N_1)^{\beta-1} + (N_1)^{\beta-1}N_2 + \ldots + (N_2)^{\beta-1} \end{bmatrix} = 0 \tag{21}$$

Based on Equation (22):

$$\begin{bmatrix} (N_1)^{\alpha-1} + (N_1)^{\alpha-1}N_2 + \ldots + (N_2)^{\alpha-1} \\ + (N_1)^{\beta-1} + (N_1)^{\beta-1}N_2 + \ldots + (N_2)^{\beta-1} \end{bmatrix} \neq 0 \tag{22}$$

Hence, it follows that $N_1 = N_2$, implying the uniqueness of f.

Hence, the proof follows.

Corollary 3

For $D_{Z_{a,b}}$ [4], it holds that:

Bulleted lists look like this:

- $\lim_{a \to 0, b \to 0} D_{Z_{a,b}} = D_R$
- $\lim_{q \to 1}\left(\lim_{a \to 0, b \to 0} D_{Z_{a,b}}\right) = D_s$
- $\lim_{a \to 1, b \to 0} D_{Z_{a,b}} = D_T$
- $\lim_{a \to k, b \to -k} D_{Z_{a,b}} = D_{Kaniadakisian\ entropy}$

- $\lim_{b\to 0} D_{Z_{a,b}} = D_{Sharma-Mittal\ entropy}$

It is worth noting that this article mainly explores the fractal dimension D_f. Having established the main theoretical foundations of D_f, it seems necessary to conduct in-depth research and search for the Ismail's entropy (IE) fractal dimension theory. So, a strong application window was necessary to look at, namely, D_f advancements in structural engineering, as follows.

4. D_f Applications to Structural Engineering

Fractal dimension crack detectors (FDCD) have been utilized to identify crack size and location in structures [16], offering valuable insights into crack characteristics with minimal data input, and extending to applications in composite plates and damage assessment in reinforced concrete structures.

Figure 5 (c.f., reference [17]) illustrates the process of detecting surface cracks using multifractal analysis, a method that quantitatively measures damage in materials like reinforced concrete shear walls. By applying the Chhabra Method of multifractal analysis to binary images taken in the visible spectrum, researchers can identify and analyze surface defects, providing valuable insights into the structural integrity of the material being studied. This approach allows for a detailed examination of crack characteristics and can be extended to various structural components for effective crack detection and analysis.

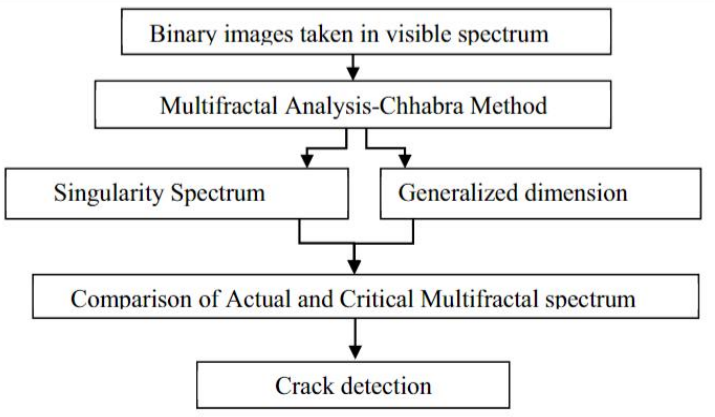

Figure 5. Detecting surface cracks using multifractal analysis.

Experimentally, four patterns were visually represented in Figure 6 (c.f., reference [16]). The study compared how each pattern deviated from the reference pattern (CASE0) based on singularity spectrum curves, showing alterations in crack shapes and growth.

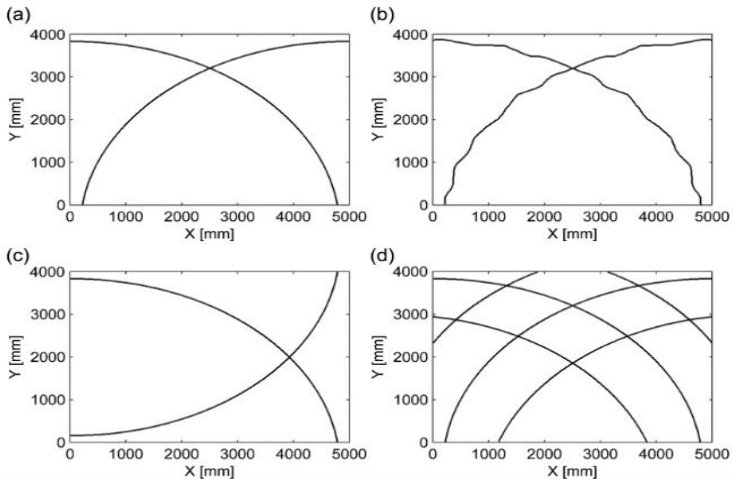

Figure 6. A singularity spectrum curves-based comparison for patterns' deviation from the reference pattern (CASE0). (**a**) CASE0; (**b**) CASE1; (**c**) CASE2; (**d**) CASE3.

In the context of the experiment, CASE0 serves as the baseline or reference pattern for the synthetic crack patterns considered. Singularity spectrum curves were used to analyze and identify cracks, as depicted in Figure 7 (c.f., reference [16]). These curves help in understanding the characteristics and variations in the crack patterns compared to the reference pattern.

This reasons how the crack patterns [16] in CASE1 closely matched those in CASE0 within a positive range of a parameter called q because the overall shape was preserved. However, in CASE2, the crack patterns were flipped, leading to a change in the overall shape and causing deviation from the base curve for negative values of q.

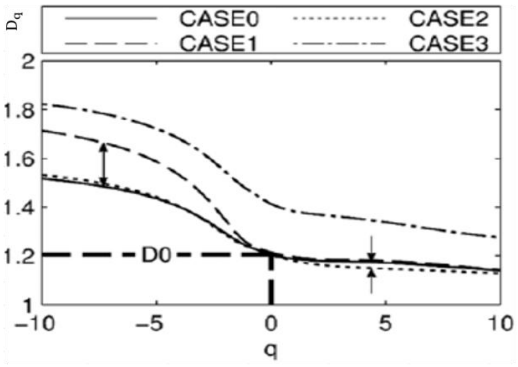

Figure 7. The significant impact of q on crack patterns.

The concept of fractals, initially explored by mathematicians like Hilbert, Mandelbrot, and others, has found applications in various fields such as plant science, neuroscience, and architecture. Fractal dimensions are used to quantify the complexity and irregularity of objects, with different values obtained based on the specific context. While deterministic fractal geometries exhibit exact self-similarity, real-life phenomena like crack patterns [18] demonstrate statistical or approximate self-similarity, as shown in Figure 8 (c.f., reference [18]).

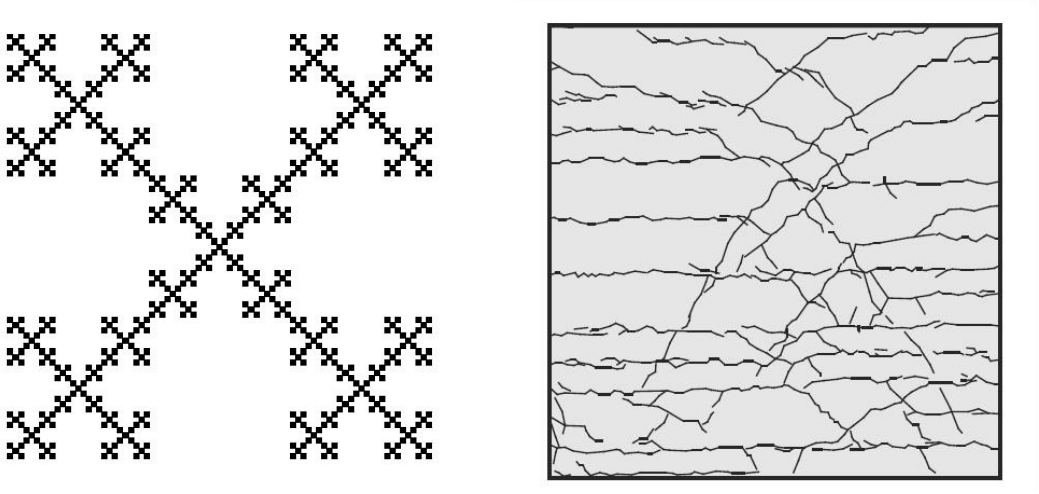

(**a**) (**b**)

Figure 8. Crack patterns from a self-similar perspective. (**a**) box fractal; (**b**) a typical crack map on a concrete wall surface.

In fractal analysis [18,19], the choice of grid position and orientation is crucial for determining the D_f of a pattern. Researchers emphasize the importance of finding the minimum number of boxes intersecting the object at each scale, which can be influenced by grid placement and orientation. Different methods, such as examining multiple positions or using optimization techniques, are employed to identify the grid configuration that minimizes the number of boxes intersecting the pattern, ultimately affecting the estimation of the fractal dimension.

In reference [20], images of crack patterns from tests on masonry and concrete walls were analyzed using AutoCAD software to create skeletonized binary representations at a scale of 1 pixel = 1 mm. A total of 83 crack maps from masonry walls and 45 crack maps from concrete walls were examined, captured at maximum drift levels and zero forces, as illustrated by Figure 9 (c.f., reference [21]).

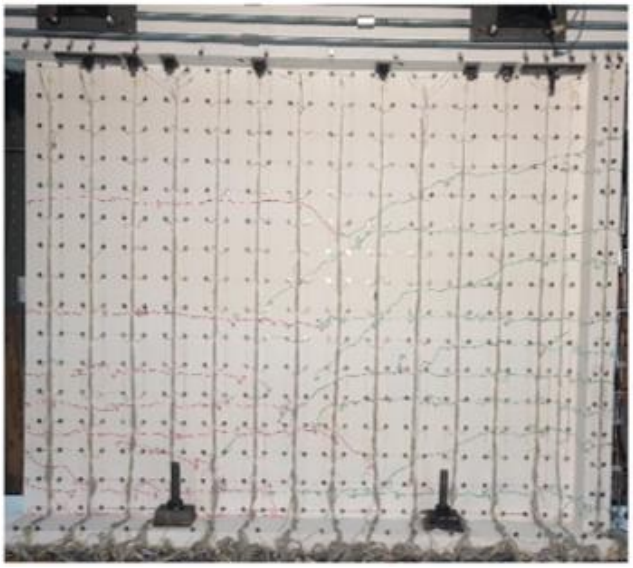

Figure 9. Crack maps from concrete walls.

Figure 10 (c.f., references [20–23]), draws a comparison that helps to understand how the choice of grid origin and orientation can impact the calculated D_f values for crack patterns in different types of walls. The study shows that these factors can lead to variations in the D_f values, especially for masonry walls, highlighting the importance of considering grid positioning in fractal analysis studies.

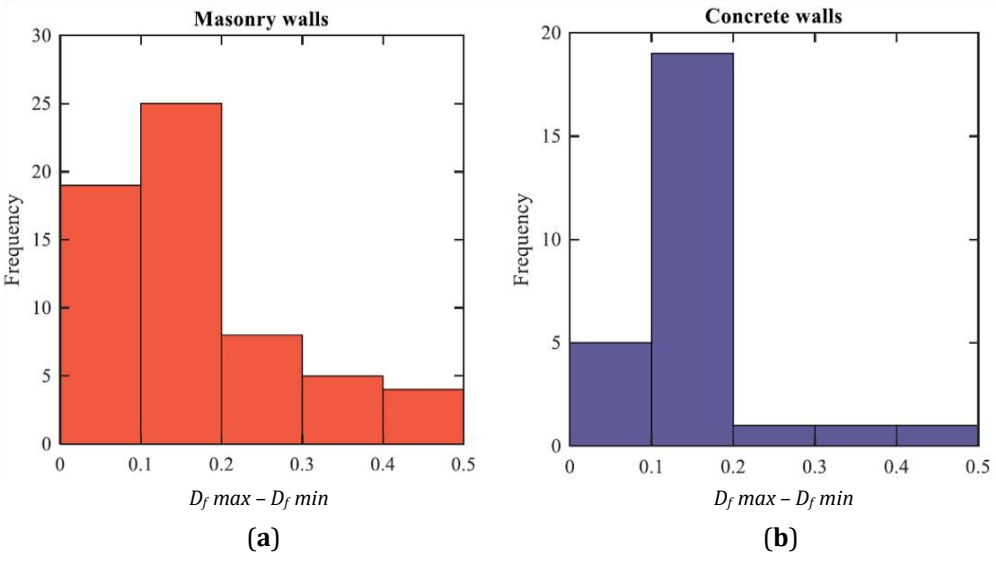

Figure 10. Comparison of the origin and orientation options for the grid can affect the D_f values computed for fracture patterns in various wall types. (**a**) D_f values for crack patterns in Masonry walls; (**b**) D_f values for crack patterns in Concrete walls.

In analyzing crack patterns in concrete walls [21], the concept of cutoffs is used to determine the fractal dimension of the cracks. The maximum cutoff value for identifying fractal behavior in concrete walls can be either 0.5 times the minimum box size (b_{min}) (Figure 11 (c.f., reference [18])) or just the minimum box size itself.

This approach helps in assessing the fractal characteristics of crack patterns in concrete structures, with 30 out of 45 crack patterns showing statistical fractal behavior in the concrete database.

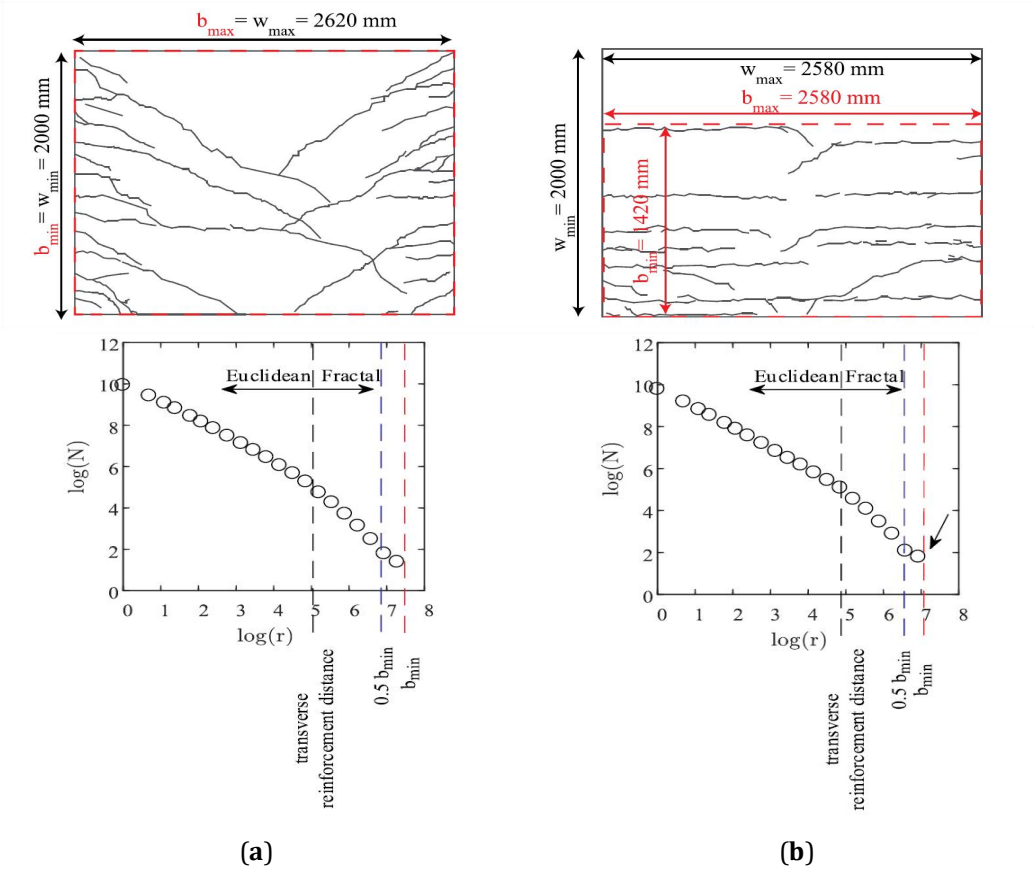

Figure 11. The concrete database's wall box size interval and breakpoint placement. (**a**) A crack map of the TW1 concrete wall at a 0.25% drift level; (**b**) A crack map showing the TW5 concrete wall at a 0.12% drift level.

This highlights [16] that crack distances align with the reinforcement spacing values. Fundamentally, this variation in crack spacing complicates the analysis of crack patterns and requires consideration of the structural elements within the concrete wall.

In analyzing crack maps [16], a change in slope in log-log plots indicates a shift in complexity, requiring reporting of two fractal dimensions to characterize the behavior. The sampling strategy [16] in the context of crack map analysis involves selecting a sequence of box sizes to evaluate the number of boxes containing cracks. Typically, a scale factor is used to determine the ratio between consecutive box sizes, ensuring enough data points for accurate analysis. In this study [21], the scale factor of was found to be optimal for evaluating crack maps, aligning with previous research on fractal geometries.

It is crucial [16] to clearly define parameters such as the scale factor, grid position, orientation, and breakpoint location to ensure accurate comparisons of fractal dimensions. This information helps characterize the size range of particles present in the gravel, which is important for understanding its properties and suitability for various applications in construction materials like mortar and concrete. By analyzing these percentages, researchers can assess the composition and quality of the crushed gravel used in their experiments or projects. This is portrayed in Figure 12 (c.f., reference [24]).

This describes adjusting the particle size distribution of marble sand to match that of river sand by specifying the mass percentages of different size ranges for the marble sand particles. This adjustment involves determining the proportions of marble sand particles within specific size intervals, such as 0.15–0.3 mm, 0.3–0.6 mm, and so on, to achieve a similar distribution to that of river sand. The data from Figure 12 (c.f., reference [24]) shows the detailed breakdown of these mass percentages for each size range of marble sand particles. This can be visualized by the actual real-life shots in Figure 13(c.f., reference [24]).

A big block of natural marble rock was first divided into smaller pieces in the experimental setting using a special saw, and the pieces were then manually broken down into stones the size of fists, as visualized by Figure 14 (c.f., reference [24]).

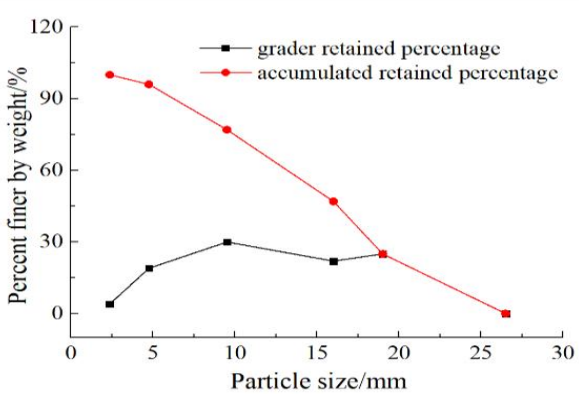

Figure 12. Relational particle size against percent finer.

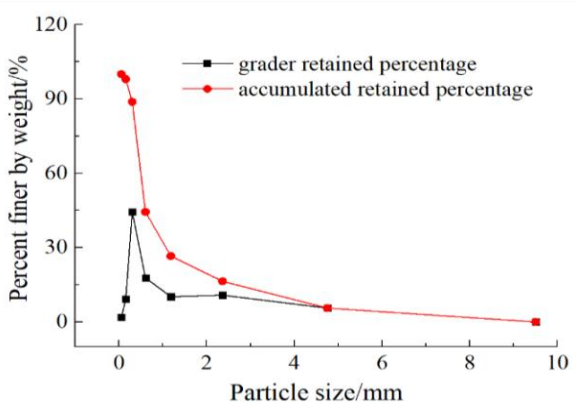

Figure 13. Fine tuning particle size against percent finer.

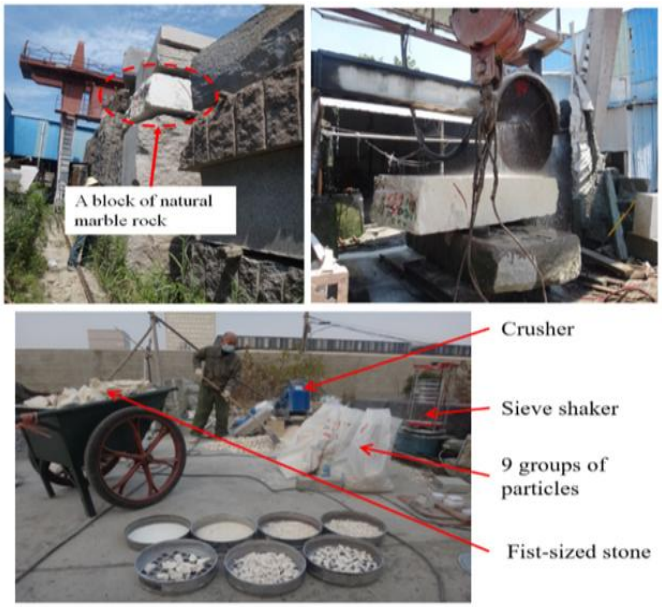

Figure 14. In the experimental setup, a large block of natural marble rock was initially cut into smaller pieces using a special saw, and then further broken down into fist-sized stones manually**.**

The process to determine concrete specimens' D_f involves using a 3D laser scanner to capture point cloud data and processing it in a matrix laboratory (MATLAB) to calculate the fractal dimension based on a method proposed by reference [25]. This method allows researchers to quantify the complex, irregular patterns on the surfaces of concrete samples, providing insights into their structural characteristics and behavior when exposed to external factors like sulfuric acid. This can be visualized and explained in Figure 15 (c.f., reference [24]).

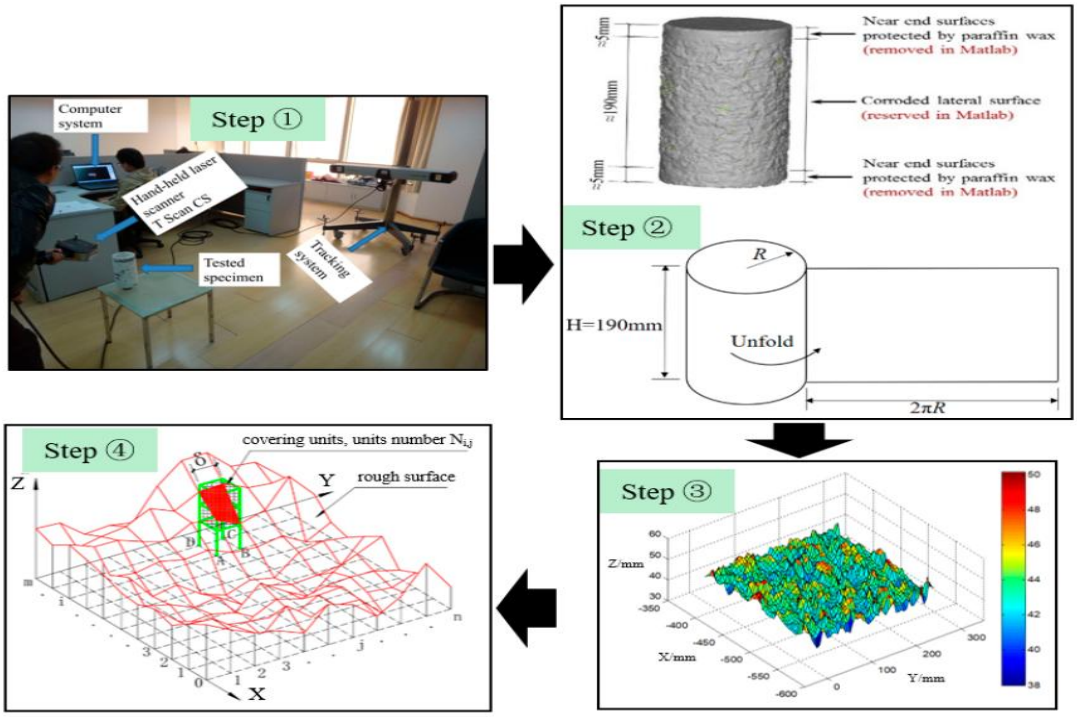

Figure 15. Fractalization of irregular patterns on the surfaces of concrete samples.

5. Conclusions, Open Problems, and Future Work

This paper reveals the dominancy of IE, especially from a fractal dimension perspective. Notably, fractal dimension applications to structural engineering are addressed.

The following are the unresolved issues:

- Can D_f (IE) threshold's formalism(c.f., Equation (8)) be computed about all the parameters involved in a mathematical challenge?
- Can we unlock the threshold of both fractal dimensions, particularly for the long-range interactions descriptor, by approaching the IE's Snow Kochflake fractal dimension (N=4 and $\varepsilon = \frac{1}{3}$) and the Sierpiniski Gasket ($N = 3$ and $\varepsilon = \frac{1}{2}$)?

It is possible to explore the frontiers to no end. Research on the open research issues as well as other new application routes for other scientific and multidisciplinary research areas will be undertaken in the next phase of the project.

Funding

This work received no external funding.

Institutional Review Board Statement

Not applicable.

Informed Consent Statement

Not applicable.

Data Availability Statement

Not applicable.

Conflicts of Interest

The authors declare no conflict of interest.

References

1. Mageed, I.A.; Zhang, Q. An Introductory Survey of Entropy Applications to Information Theory, Queuing Theory, Engineering, Computer Science, and Statistical Mechanics. In Proceedings of the 2022 27th International Conference on Automation and Computing, Bristol, UK, 1–3 September 2022. [CrossRef]
2. Mageed, I.A.; Zhang, Q. An Information Theoretic Unified Global Theory for a Stable *M/G/*1 Queue with Potential Maximum Entropy Applications to Energy Works. In Proceedings of the 2022 Global Energy Conference, Batman, Turkey, 26–29 October 2022. [CrossRef]
3. Kouvatsos, D.D.; Mageed, I.A.; Anisimov, V.; Limnios, N. Non-extensive Maximum Entropy Formalisms and Inductive Inferences of Stable M/G/1 Queue with Heavy Tails. *Adv. Trends Queue. Theory* **2021**, *2*. [CrossRef]
4. Mageed, I.A.; Bhat, A.H. Generalized Z-Entropy (Gze) and Fractal Dimensions. *Appl. Math. Inf. Sci.* **2022**, *16*, 829–834. [CrossRef]
5. Zhou, L.; Johnson, C.R.; Weiskopf, D. Data-Driven Space-Filling Curves. *IEEE Trans. Visualization Comput. Graphics* **2020**, *27*, 1591–1600. [CrossRef]
6. Wang, W.J.; Xu, X.; Shao, Y.; Liao, J.W.; Jian, H.X.; Xue, B.; Yang, S.G. Fractal Growth of Giant Amphiphiles in Langmuir-Blodgett Films. *Chin. J. Polym. Sci.* **2022**, *40*, 556–566. [CrossRef]
7. Sadem, Z.; Fathi, B.; Mustapha, L. Image Edge Detection and Fractional Calculation. *Int. J. Adv. Nat.Sciences Eng. Res.* **2023**, *7*, 222–225.
8. Nayak, S.R.; Mishra, J. Analysis of medical images using fractal geometry. In *Research Anthology on Improving Medical Imaging Techniques for Analysis and Intervention*; Medical Information Science Reference; IGI Global: Hershey, PA, USA, 2023; pp. 1547–1562. [CrossRef]
9. Gao, X.L.; Shao, Y.H.; Yang, Y.H.; Zhou, W.X. Do the Global Grain Spot Markets Exhibit Multifractal Nature? *Chaos, Solitons Fractals* **2022**, *164*, 112663. [CrossRef]
10. Zhao, T.; Li, Z.; Deng, Y. Information Fractal Dimension of Random Permutation Set. *Chaos, Solitons Fractals* **2023**, *174*, 113883. [CrossRef]
11. Pons, F.; Messori, G.; Faranda, D. Statistical Performance of Local Attractor Dimension Estimators in Non-Axiom A Dynamical Systems. *Chaos: An Interdiscip. J. Nonlinear Sci.* **2023**, *33*. [CrossRef]
12. Mageed, I.A.; Zhang, Q. The Rényian-Tsallisian Formalisms of the Stable M/G/1 Queue with Heavy Tails Entropian Threshold Theorems for the Squared Coefficient of Variation. *Electron. J. Comput. Sci. Inf. Technol.* **2023**, *9*, 7–14.
13. Mageed, I.A.; Zhang, Q. Inductive Inferences of Z-Entropy Formalism (ZEF) Stable M/G/1 Queue with Heavy Tails. In Proceedings of the 2022 27th International Conference on Automation and Computing, Bristol, UK, 1–3 September 2022. [CrossRef]
14. Mageed, I.A. Fractal Dimension (Df) Theory of Ismail's Second Entropy (H_1^q) with Potential Fractal Applications to ChatGPT, Distributed Ledger Technologies (DLTs) and Image Processing (IP). In Proceedings of the 2023 International Conference on Computer and Applications, Cairo, Egypt, 28–30 November 2023. [CrossRef]
15. Mageed, I.A. Fractal Dimension (Df) of Ismail's Fourth Entrop ($H_{IV}^{(q,a_1,a_2,\ldots,a_k)}$) with Fractal Applications to Algorithms, Haptics, and Transportation. In Proceedings of the 2023 International Conference on Computer and Applications, Cairo, Egypt, 28–30 November 2023. [CrossRef]
16. Anwar, A.; Adarsh, S. A Review on Fractal Analysis and its Applications in Structural Engineering. In Proceedings of the IOP Conference Series: Materials Science and Engineering, Kerala, India, 14–15 July 2020. [CrossRef]
17. Ebrahimkhanlou, A.; Farhidzadeh, A.; Salamone, S. Multifractal Analysis of Crack Patterns in Reinforced Concrete Shear Walls. *Struct. Health Monit.* **2016**, *15*, 81–92. [CrossRef]
18. Rezaie, A.; Mauron, A.J.; Beyer, K. Sensitivity Analysis of Fractal Dimensions of Crack Maps on Concrete and Masonry Walls. *Automation Const.* **2020**, *117*, 103258. [CrossRef]

19. Feldman, D.P. *Chaos and Fractals: An Elementary Introduction*, 1st ed.; Oxford University Press: Oxford, UK, 2012. [CrossRef]
20. Almeida, J.; Prodan, O.; Rosso, A.; Beyer, K. Tests on Thin Reinforced Concrete Walls Subjected to in-Plane and Out-of-Plane Cyclic Loading. *Earthquake Spectra* **2017**, *33*, 323–345.
21. Autodesk Education Resources. Available online: http://students.autodesk.com/ (accessed on 25 July 2024).
22. Petry, S.; Beyer, K. Cyclic Test Data of Six Unreinforced Masonry Walls with Different Boundary Conditions. *Earthquake Spectra* **2015**, 31, 2459–2484.
23. Petry, S.; Beyer, K. Scaling Unreinforced Masonry for Reduced-Scale Seismic Testing. *Bull. Earthquake Eng.* **2014**, *12*, 2557–2581. [CrossRef]
24. Xiao, J.; Long, X.; Li, L.; Jiang, H.; Zhang, Y.; Qu, W. Study on the Influence of Three Factors on Mass Loss and Surface Fractal Dimension of Concrete in Sulfuric Acid Environments. *Fractal Fract.* **2021**, *5*, 146. [CrossRef]
25. Zhou, H.W.; Xie, H. Direct Estimation of the Fractal Dimensions of a Fracture Surface of Rock. *Surf. Rev. Lett.* **2003**, *10*, 751–762. [CrossRef]